Metal-gate-induced reduction of the interfacial layer in Hf oxide gate stacks

L. V. Goncharova,[a] M. Dalponte, and T. Gustafsson
Department of Physics and Astronomy, and Laboratory for Surface Modification, Rutgers University, 136 Frelinghuysen Rd., Piscataway, New Jersey 08854

O. Celik and E. Garfunkel
Department of Chemistry and Chemical Biology, and Laboratory for Surface Modification, Rutgers University, 610 Taylor Rd., Piscataway, New Jersey 08854

P. S. Lysaght and G. Bersuker
SEMATECH, 2705 Montopolis Dr., Austin, Texas 78741

(Received 18 October 2006; accepted 28 December 2006; published 13 February 2007)

The properties of high-κ metal oxide gate stacks are often determined in the final processing steps following dielectric deposition. We report here results from medium energy ion scattering and x-ray photoelectron spectroscopy studies of oxygen and silicon diffusion and interfacial layer reactions in multilayer gate stacks. Our results show that Ti metallization of $HfO_2/SiO_2/Si$ stacks reduces the SiO_2 interlayer and (to a more limited extent) the HfO_2 layer. We find that Si atoms initially present in the interfacial SiO_2 layer incorporate into the bottom of the high-κ layer. Some evidence for Ti–Si interdiffusion through the high-κ film in the presence of a Ti gate in the crystalline HfO_2 films is also reported. This diffusion is likely to be related to defects in crystalline HfO_2 films, such as grain boundaries. High-resolution transmission electron microscopy and corresponding electron energy loss spectroscopy scans show aggressive Ti–Si intermixing and oxygen diffusion to the outermost Ti layer, given high enough annealing temperature. Thermodynamic calculations show that the driving forces exist for some of the observed diffusion processes. © *2007 American Vacuum Society.*
[DOI: 10.1116/1.2435376]

I. INTRODUCTION

Scaling of the gate stack in silicon metal-oxide-semiconductor-field-effect-transistors (FETs) is one of the key challenges in microelectronics today. Two crucial material issues that need to be resolved concern the gate oxide (where SiON dielectrics need to be replaced with a higher dielectric constant material, such as HfO_2) and the metallic gate electrode (where doped polysilicon will need to be replaced by a metal). For the latter case, the metals should satisfy several requirements, including suitable effective work functions, thermodynamic stability next to the high-κ layers at temperatures required for complementary metal oxide semiconductor processing, ability to act as a diffusion barrier, and a well defined, controllable microstructure. Gate metals with two different work functions will be required for the *p*- and *n*-FETs. Several metals have been explored recently as candidates for such use.[1–4]

When metals are deposited on a HfO_2 (or Hf silicate)/SiO_2/Si stack, additional interactions may occur both at the metal/high-κ and high-κ/Si interfaces, that may either improve or degrade electrical device performance. Interfacial reactions or interdiffusion that occurs during high temperature processing may result in changes in capacitance of the dielectric, defect concentrations, the threshold voltage, and/or the leakage current. What actually happens in each specific case depends on the chemical nature of the gate metal and its thermal stability in the presence of the high-κ dielectric layer.[5] Crystallite grain growth or nanostructure changes at high annealing temperatures may roughen the metal gate/high-κ interface, leading to changes in the work function of the metal and nonuniformity of the field seen by the carriers. Intrinsic defects, such as oxygen vacancies or interstitials,[6,7] can also initiate diffusion and additional interface reactions. Defects can furthermore be the centers of voltage-dependent charge trapping and degrade the mobility of the device or the threshold voltage.

Several metals have been investigated that modify the behavior of the overall gate stack.[1,8–11] It was shown by Preisler *et al.*[8] that in W/HfO_2 gate stacks the tungsten can under certain conditions introduce excess oxygen, resulting in interfacial SiO_2 growth at the HfO_2/Si interface. In contrast, Ti appears to act as an oxygen getter when used as a gate metal on HfO_2/SiO_2 and ZrO_2/SiO_2 dielectric stacks.[12] This was attributed to the very high oxygen solubility in Ti, which leads to oxygen extraction from the SiO_2 interface interlayer through the metal oxide high-κ layer, thus decomposing the interfacial SiO_2. One can surmise that the O concentration (activity) in and above the metal layer will affect its tendency to oxidize or to reduce neighboring layers such as the dielectric. TiN, a midgap metal, was found to behave similarly to Ti, acting as an oxygen sink after thermal treatment.[9] Hf, Ti, and N interdiffusion at the TiN/HfO_2 interface has been reported by some authors,[2] whereas others report a thermally stable interface but with significant roughening.[13] Electron microscopy studies revealed significant roughening at both TiN/HfO_2 and HfO_2/SiO_2 interfaces and possible protrusion of Hf into the interfacial SiO_2

[a]Electronic mail: lgoncha@physics.rutgers.edu

layer.[9,14] The latter effect has been suggested as being correlated with the apparent high permittivity of the interfacial SiO_x layer (between HfO_2 and Si) compared to pure SiO_2. Studies of $HfO_2/SiO_xN_y/Si$ structures[10] metallized by Re show the reduction of the HfO_2 and Hf silicate to a suboxide during postmetal deposition annealing in vacuum. Also, significant electrostatic shifts were reported due to charged defects, tentatively attributed to oxygen vacancies.

Our work follows the Ti overlayer oxygen gettering study by Kim *et al.*,[12] with the emphases on examining different diffusion processes and the behavior of individual layers in $Ti/HfO_2/SiO_2/Si$ structures as a function of annealing temperature and of the crystallization state of the HfO_2 layers prior to metallization, using the high-resolution elemental profiling capability of medium energy ion scattering (MEIS). MEIS was used to determine oxygen areal densities and oxygen and silicon elemental depth profiles. In addition, the chemical states of the Ti, Si, and Hf atoms were studied by x-ray photoelectron spectroscopy (XPS), the surface roughness of selected samples was monitored by atomic-force microscopy (AFM). Ti metallization and annealing were conducted *in situ* and were followed by MEIS at each step. This allows us to determine the composition of each layer and both high-κ/Si and metal gate/high-κ interfaces. We examined the conditions for oxygen dissolution into the Ti layer resulting in the decomposition and thinning of interfacial SiO_2. Ti–Si interdiffusion was confirmed by high-resolution transmission electron microscopy (HRTEM) and electron energy loss spectroscopy (EELS) on the separate set of samples with thicker Ti/TiN layers. A scenario for the Si diffusion and incorporation that remain after SiO_2 reduction is proposed, and the possibility of HfO_2 layer reduction is also considered.

II. EXPERIMENT

The HfO_2 films were deposited *ex situ* on a 1 nm $SiO_2/Si(001)$ film using atomic layer deposition at 325 °C with O_3 as an oxidation agent and tetrakis (ethylmethylamino) hafnium precursor. The details of the deposition process were described in detail previously.[15] Selected $HfO_2/SiO_2/Si$ stacks then underwent UHV crystallization annealing[16] at 750 °C for 40 min. These films are referred to as cryst-$HfO_2/SiO_2/Si$ below. All as-deposited films were annealed briefly to ~250 °C before analysis to eliminate hydrocarbon surface contamination. Titanium deposition was performed using a titanium evaporation source in an UHV chamber (base pressure $\sim 10^{-9}$ Torr), and then transferred in vacuum into the adjacent MEIS chamber for characterization.

Compositional depth profiles were obtained using MEIS, a low energy, high-resolution version of Rutherford backscattering spectroscopy. The excellent depth resolution of MEIS is due to the use of a toroidal electrostatic energy analyzer[17] and the fact that the stopping power for protons in silicon has its maximum in the 100 keV energy range.[18] A slightly higher H^+ energy (130.3 ± 0.1 keV in our case) was used to achieve a better separation between oxygen isotope peaks. Depth profile information is deduced from the energy distribution of the backscattered ions. Knowledge of the cross section, the ion stopping power, and the energy straggling allows us to deconvolute the energy distribution into a concentration versus depth profile, assuming that the film's density is known or can be calculated. Quantitative depth profiles for different species are extracted with a resolution of 3–5 Å in the near-surface region, with somewhat worse resolution for the deeper layers due to ion straggling. Note that all MEIS data represent averages over a sample area ($\sim 1-10$ mm^2); this makes it difficult for us to distinguish between a near-interface compositional gradient and interface or surface roughness. A double-aligned scattering geometry was used in all measurements with the ion beam normal to the Si (001) surface and the detector aligned with the {111} Si direction (a scattering angle of 125.26°).

XPS and AFM measurements were conducted *ex situ*. A commercial XPS system (PHI 5000 series ESCA spectrometer, Al/Mg dual anode source, concentric hemispherical analyzer) was used with a photoelectron take-off angle of 45° and using Al $K\alpha$ radiation (1486.6 eV). The instrument was calibrated with the Au $4f_{7/2}$ level at 83.9 eV. Charging, when present, was corrected by referencing the energy scale to the C1*s* peak to 285 eV. After a Shirley background subtraction, the spectra were fitted with Gaussian peaks using a minimum deviation curve fitting method (SPECTRAL DATA PROCESSING software, version 4).

The evolution of the surface morphology due to annealing after Ti deposition was studied by AFM (Digital Instruments Nanoscope IIIA, equipped with J scanner). Images were taken under ambient conditions in the "tapping" mode using 125 μm long silicon cantilevers with resonant frequencies ~250 kHz. Large scale image curvature from the piezoelectric scanners was removed using WSXM2.2 software developed by Nanotec Electronica SL.

HRTEM and corresponding EELS were utilized to compare $TiN/Ti/HfO_2/SiO_2/Si$ samples before and after rapid (10 s long) annealing to 1000 °C in dry N_2 atmosphere with thicker TiN/Ti layers (100–400 Å Ti/400 Å TiN). EELS and energy-dispersive x-ray spectroscopy (EDXS) data were recorded in scanning transmission electron microscopy (STEM) mode while stepping small focused electron probes of ~3 and ~5 Å in diameter, respectively, across the layers comprising the gate stack. In STEM, the atomic-resolution image is formed by scanning a focused electron beam (a few angstroms in diameter) and collecting the electrons on an annular dark field (ADF) detector. The image contrast in ADF is roughly proportional to Z^2 (atomic number),[19] and provides the additional benefit of a chemically sensitive image for thin samples.[20] Profiles were generated by extracting spectral counts by integration of spectra over selected energy ranges after appropriate background subtraction.

III. RESULTS

An analysis of the MEIS spectra of the as-deposited HfO_2 films (Fig. 1) shows the existence of a small amount of interfacial SiO_2 (~6–7 Å). The bulk of the Hf oxide layer is

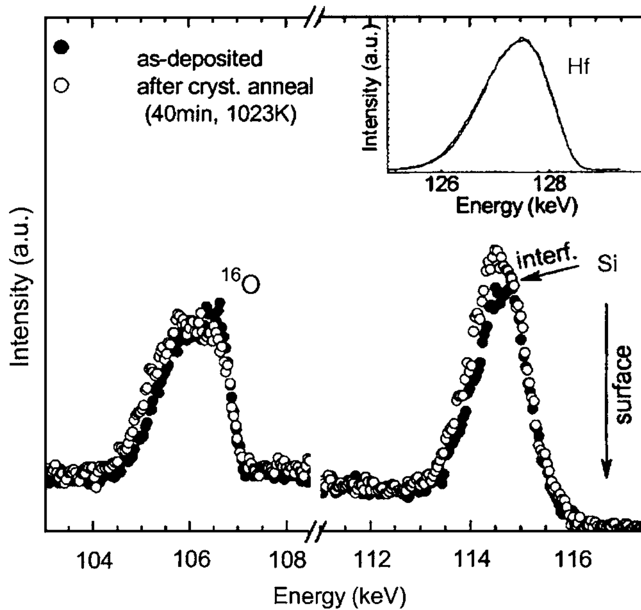

FIG. 1. MEIS spectra for a $HfO_2/SiO_2/Si(001)$ stack before (dark circles) and after crystallization annealing (open circles). Note the absence of the surface Si peak and no significant changes in the Hf peak (see the insert). An incident proton energy of 130.3 keV was used with the incident direction normal to the surface and the detector aligned at 125.3° scattering angle.

slightly oxygen rich ($\sim HfO_{2.07}$); this may be due to incorporated interstitial oxygen atoms during deposition (trapped H_2O or –OH are less likely in this case as the oxidant is O_3). After a crystallization anneal at 750 °C, additional interfacial SiO_2 growth is observed in the MEIS spectra as an increase in the size of the Si peak (corresponding to additional disordered Si atoms) and a broadening of the O peak (corresponding to O atoms at a greater depth). At the same time, the oxygen content in the high-κ film is reduced, making its composition closer to stoichiometric HfO_2. Absence of the surface Si peak (Fig. 1, at 116.4 keV) for both as-deposited and crystallized films shows that there is no segregated Si on the topmost HfO_2 surface and that the Si concentration is below 0.3×10^{15} at./cm^3 inside the HfO_2 layer.

Backscattering spectra for an as-deposited $HfO_2/SiO_2/Si$ stack after 4.2 nm Ti deposition and after a subsequent anneal to 300 °C in UHV are presented in Fig. 2(a). The Hf, Si, and interface O peaks are shifted from their surface energy peak positions to lower energies, due to energy loss in the Ti layer. Simulations for a $HfO_2/SiO_2/Si$ stack after Ti deposition [Fig. 2(b)] confirm that the Ti layer thickness is uniform. A distinct surface O peak ($\sim$106 keV) and the low O yield between the surface and interface peaks (106–107 keV) show that the oxygen concentration in the Ti layer is small ($Ti-O_x$, $x<0.10$), with enhanced oxidation occurring at the surface (2–3 Å of Ti_2O_3) and at the Ti/HfO_2 interface (5 Å of TiO_x, $0.5<x<1$). (Note that Ti reactions with the background gases in the UHV chamber cannot be totally neglected.) Comparisons with simulations show that the Si areal density remains the same after Ti deposition, while the interfacial O areal density decreases. This comparison of the Si and O peaks and a full analysis of the experimental spectra indicate that the original SiO_2 likely remains at the $HfO_2/Si(001)$ interface; however, there is a partial depletion of oxygen in the HfO_2 layer. Note again that the as-deposited HfO_2 layer contains excess oxygen in it. Additional measurements with other techniques will be necessary to conclude whether this oxygen diffusion from the Hf oxide layer into the Ti overlayer creates a stoichiometric HfO_2 layer or if it also creates oxygen vacancies[7,21] in the HfO_2 layer ($V_{O,HfO2}$):

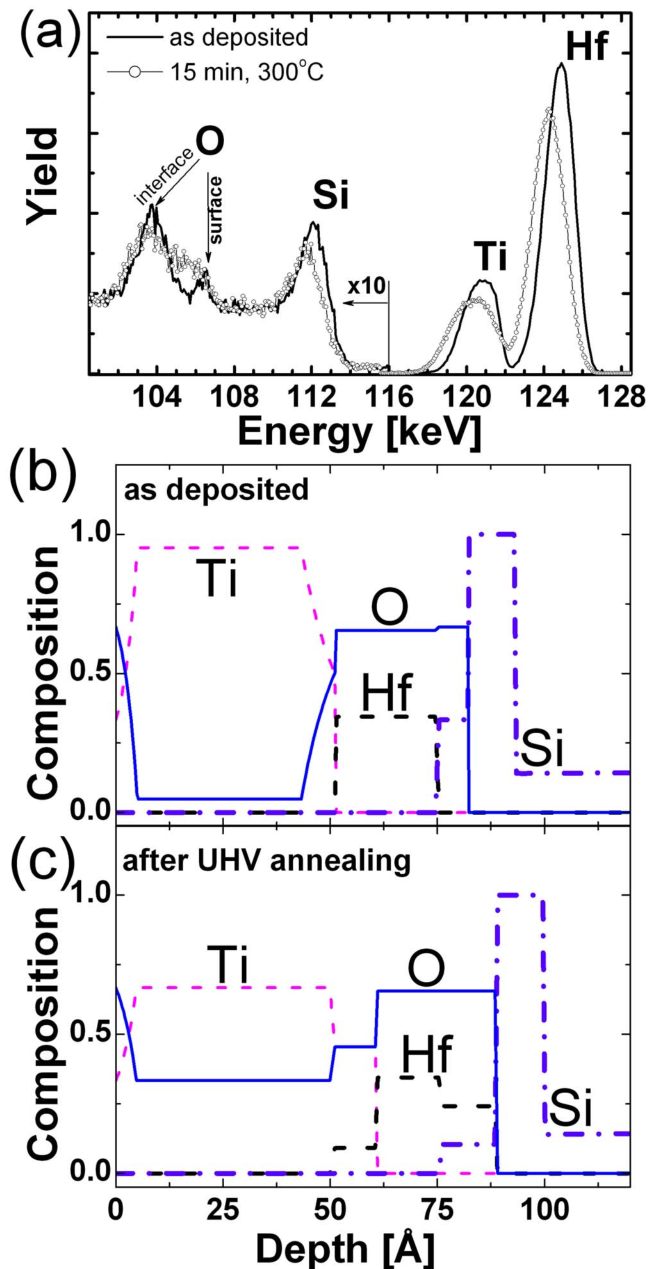

FIG. 2. (a) Medium energy ion spectra for a $Ti/HfO_2/SiO_2/Si(001)$ stack directly after metal deposition (solid line) and subsequent to a 300 °C UHV annealing (open symbols). [(b) and (c)] Best fit depth profiles for Ti, Hf, Si, and O.

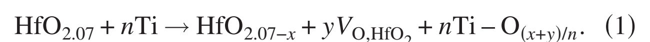

$$HfO_{2.07} + n\mathrm{Ti} \rightarrow HfO_{2.07-x} + yV_{O,HfO_2} + n\mathrm{Ti}-O_{(x+y)/n}. \quad (1)$$

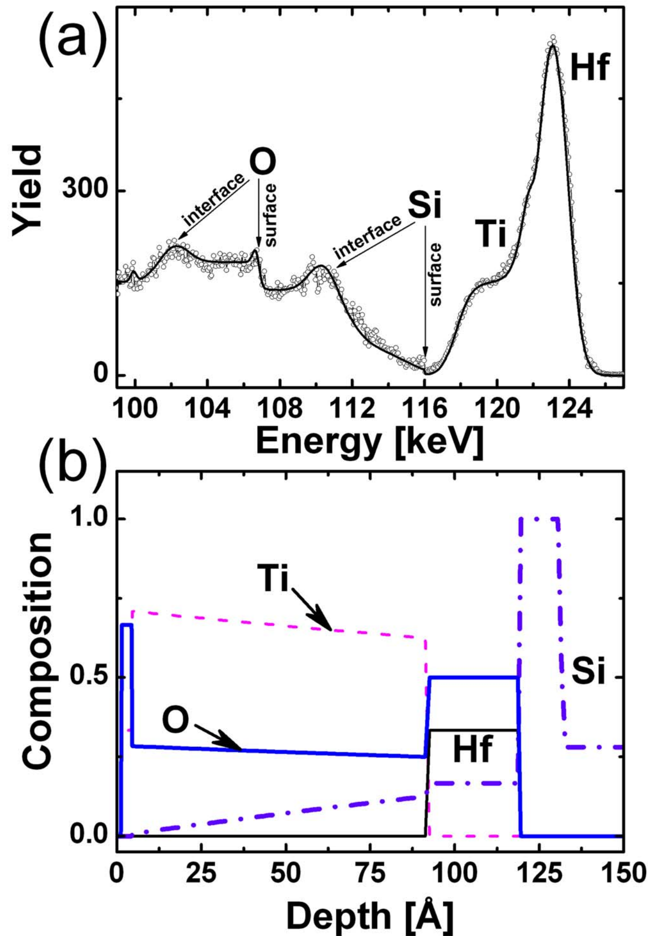

FIG. 3. (a) Backscattering spectra of the Ti/cryst-$HfO_2/SiO_2/Si(001)$ stack after 300 °C UHV annealing. (b) Depth profiles for Ti, Hf, Si, and O used in the fit of the experimental data.

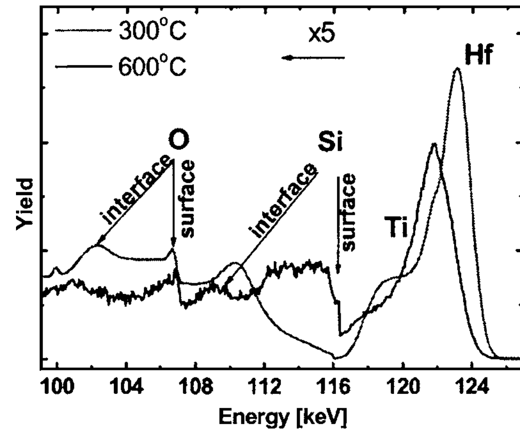

FIG. 4. Comparison of MEIS spectra for the Ti/cryst-$HfO_2/SiO_2/Si(001)$ stack annealed at 300 °C and at 600 °C.

After a UHV anneal of the Ti/HfO_2/SiO_2/Si stack we observe lowering and broadening of the Ti peak concurrent with growth of the O yield in the Ti layer, indicative of more oxygen incorporation into the Ti layer (up to $TiO_{0.5}$). In general case oxygen incorporation into Ti may result either in O dissolution in Ti (Ti–O_x alloy formation under oxygen deficient condition), or in Ti oxide compound formation. Our experimental MEIS profiles indicate that the amount of O incorporated into the bulk of Ti overlayer (TiO_x) never exceeds the O solubility limit in Ti (X_{limit}=0.49).[22] The O content is larger (above the solubility limit) at the Ti/HfO_2 interface, as presented in the composition depth profile [Fig. 2(c)], suggesting titanium oxide formation with mixed Ti oxidation state. At the same time, the decrease of the Si peak and narrowing of the O peak are consistent with *partial removal of the interfacial SiO_2 layer*. The amount of SiO_2 reduction is, as one might expect, dependent on the Ti layer thickness. Assuming that all the oxygen from SiO_2 goes into the Ti–O alloy overlayer (Ti–$O_{0.49}$),[23] one can estimate that in order to reduce 7 Å of SiO_2, a minimum Ti layer thickness of 28.6 Å is necessary. The Si and Hf MEIS data imply that some of the Si initially present in the interfacial SiO_2 layer incorporates in the high-κ layer (i.e., not all of it recrystallizes as part of the substrate Si).

Exposure of the UHV annealed stack to air (for up to ~12 h) results in no significant changes. Although the surface Ti layer oxidizes further, oxidation of the bulk of Ti film to TiO_2 is not achieved.

When Ti is deposited on the cryst-HfO_2/SiO_2/Si stack, somewhat different behavior is observed than noted above for the unannealed sample. Directly after Ti deposition, the cryst-HfO_2/SiO_2/Si stack behaves similar to the as-deposited HfO_2 films. However, after UHV annealing at $T \geqslant 300$ °C, differences are observed: in addition to O diffusion into the Ti layer, we also see a shift of the high-energy edge of the Si peak to the higher energy (~114 keV, Fig. 3). This change in Si profile corresponds to (limited) Si diffusion into the HfO_2 and TiO_x layers. Note, however, that the Si does not reach the outer surface, as the surface Si peak position is at ~116.4 keV. The absence of a surface Si peak also argues against the development of cracks throughout both the TiO_x and the HfO_2 layers under these annealing conditions. After a $\geqslant$500 °C anneal, a surface Si peak appears (Fig. 4) and the overall lateral inhomogeneity of the sample indicates either the opening of cracks in TiO_2/HfO_2 layers or further Si diffusion with possible Ti–Si and Ti–Si–O phases formation. Note that while the Hf peak shape changes, the position of its high-energy edge does not shift to the energy characteristic of Hf at the surface (~128.2 keV). Thus Hf diffusion into the Ti layer is not observed. The Hf layer stays covered by Ti, hence only Ti, O, and Si exist at the outer surface.

The change in the surface morphology is quite clear from the AFM topographs, which show that while the surfaces of the initial as-deposited and cryst-$HfO_2/SiO_2/Si(001)$ stacks are basically flat [Fig. 5(a)], after Ti deposition and UHV annealing, the roughness increases [Fig. 5(b)]. In addition, a variety of topographic features is observed on the surface after a 500–600 °C anneal: round voids ~1 nm deep (not shown), centered islands 1–1.5 nm high [a cross section is shown in Fig. 5(c), A], and small particles ~5–10 nm high (not shown). The lateral size of the islands varies from

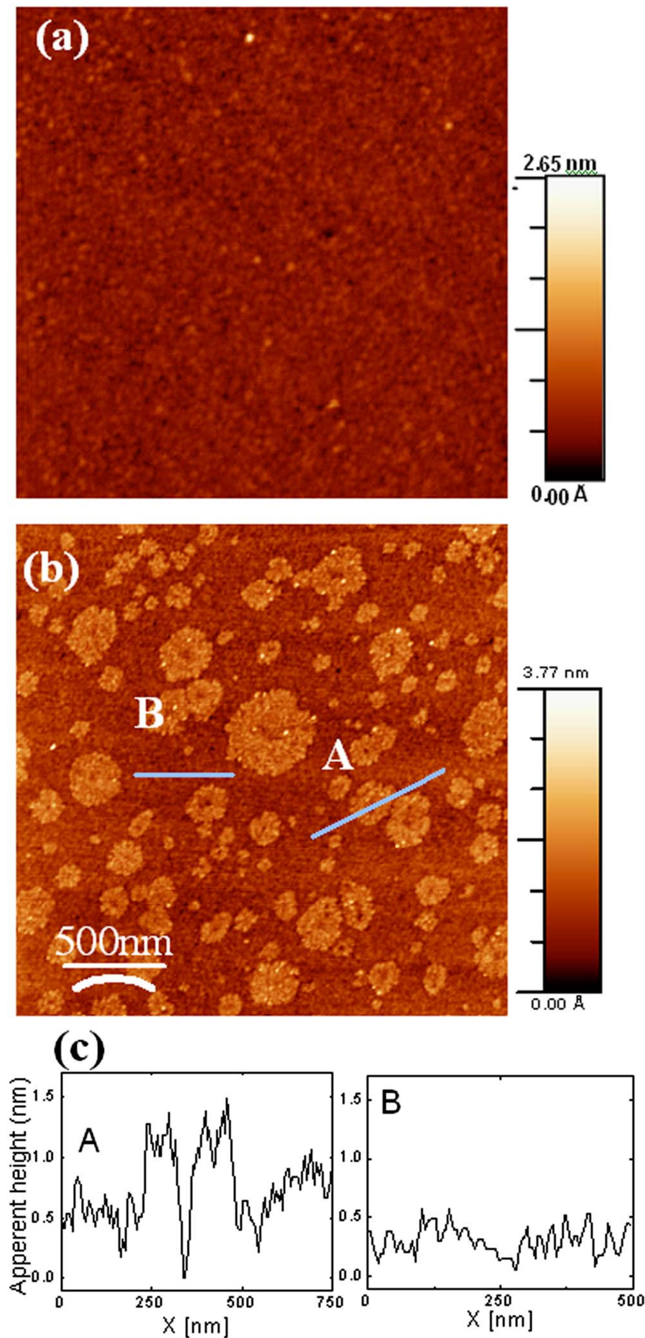

FIG. 5. AFM topography of the HfO_2 films (a) after recrystallization annealed at 750 °C, rms roughness 1 Å ($a > 5$ nm diameter probe tip was used, note that the use of the smaller (<1 nm) tip can reveal the surface topography more accurately); (b) after Ti deposition and annealed ~500 °C, rms roughness 3 Å. The scanned area is 2.5×2.5 μm^2 (c) Z profile through the A and B lines in (b).

50 to 500 nm. It is important to point out that each of the centered islands has a round shape with an opening in the middle, possibly a nucleation center for the island evolution. The bottom of this opening can be estimated to be on the same vertical height as the flat part of the surface or even below that level [Fig. 5(c), A and B]. As these islands appear only after 500–600 °C annealing, based on the MEIS results discussed above and the XPS data presented next, we can tentatively propose that their chemical composition is $TiSi_x$ (or $TiSiO_y$ after the air exposure). The nature of the small particles [not shown in Fig. 5(b)] has yet to be understood.

Selected XPS results are shown in Fig. 6 with a deconvolution of the Ti 2p XPS peak into several components in Fig. 6(a). Both large contributions from metallic Ti (454.2 eV), TiO_2 (458.9 eV) as well as minor ones from TiO (455.6 eV) and Ti_2O_3 (457.4 eV) can be observed. These values agree very well with those reported in the literature.[24–27] The peak at 460.2 eV is tentatively assigned to a relaxation effect due to TiO_2 mixing with SiO_2. (TiO_2 mixing with HfO_2 cannot explain this shift, as the Ti 2p peak position at 458.5 eV was reported[28] in $HfTiO_4$ films on Si.) A similar shift has also been observed in bulk titanium silicates[29] and zirconium silicate[30] thin films. Generally, larger chemical shifts are expected to be observed in a complex $A_xM_yO_z$ oxide compared to a simple A_xO oxide (where A_xO is an *ionic* oxide and M_yO is a *covalent* oxide[31]) due to enhanced A_xO ionicity and hence higher oxygen coordination in $A_xM_yO_z$.

Comparison of the Si 2p peaks for pure HfO_2 films shows that after the crystallization annealing the amount of interfacial SiO_2 slightly increases, consistent with our MEIS observations [Fig. 6(b)]. After Ti deposition and annealing, both Si^0 and Si^{4+} components grow, showing elemental Si and its oxidized compounds at the surface and in the near-surface layer, possibly as a mixture of Ti silicide, Si, and SiO_2.

The Hf 4f doublet is observed at 18.6 and 16.9 eV, characteristic of fully oxidized Hf (Hf^{4+}).[32] The Hf 4f intensity becomes substantially smaller after Ti deposition [Fig. 6(c), no change after crystallization annealing], confirming that the HfO_2 layer is covered with titanium. The HfO_2 layer is now partially reduced, as seen from a small shift (~0.2 eV) of the Hf 4f doublet, closer to the metallic Hf peak position, and the appearance of a shoulder on the low energy edge of the doublet.

Significant Ti–Si interdiffusion after 1000 °C/10 s/N_2 annealing is illustrated by HR-STEM results [Fig. 7(a)]. The z-contrast images reveal formation of relatively high z Hf-containing islands (bright spots). Choosing to scan linearly through a region avoiding the bright spots would detect little or no Hf. EELS elemental profiles through selected line show Si diffusion up into Ti layer. At the same time Ti diffusion into the Hf layer and even below is also detected [Fig. 7(b)].

IV. DISCUSSION

Oxygen diffusion via lattice oxygen exchange[33,34] in Hf- and Zr-based dielectrics is well known. The fact that the oxygen (and oxygen vacancy) mobility is high in HfO_x and the strong affinity of Hf for oxygen has been correlated with a reduction of the interfacial SiO_2 during metallic Hf deposition in $Hf/HfO_2/SiO_2/Si$ stacks.[6] Conversely, interstitial O^{2-} and OH^- species incorporated in HfO_2 during film growth can cause additional SiO_2 growth during postprocessing, as shown both by calculations[35] and experiment.[36] Decomposition of the native SiO_2 layer after direct Ti deposi-

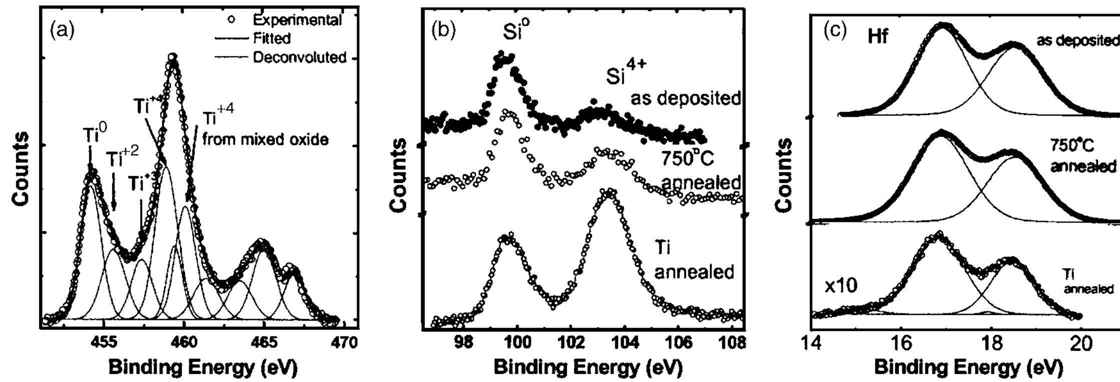

FIG. 6. XPS data in the (a) Ti $2p$, (b) Si $2p$, and (c) Hf $4f$ regions from $HfO_2/SiO_2/Si(001)$. The deconvolutions of the Ti peak due to different TiO_x contributions are shown by the thin lines. The Si $2p$ spectra are normalized to the Si^0 peak.

tion has been also demonstrated.[37,38] When a Ti overlayer is in contact with HfO_2, a possible set of solid phase reactions can be described by the following equations:

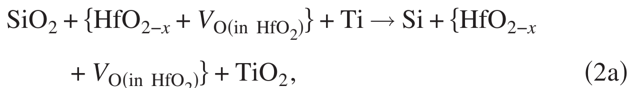

$$SiO_2 + \{HfO_{2-x} + V_{O(\text{in } HfO_2)}\} + Ti \rightarrow Si + \{HfO_{2-x} + V_{O(\text{in } HfO_2)}\} + TiO_2, \tag{2a}$$

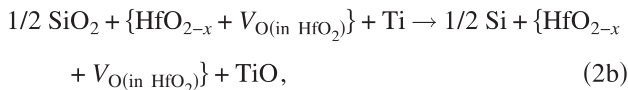

$$1/2\ SiO_2 + \{HfO_{2-x} + V_{O(\text{in } HfO_2)}\} + Ti \rightarrow 1/2\ Si + \{HfO_{2-x} + V_{O(\text{in } HfO_2)}\} + TiO, \tag{2b}$$

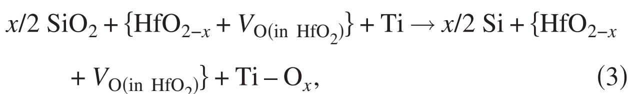

$$x/2\ SiO_2 + \{HfO_{2-x} + V_{O(\text{in } HfO_2)}\} + Ti \rightarrow x/2\ Si + \{HfO_{2-x} + V_{O(\text{in } HfO_2)}\} + Ti - O_x, \tag{3}$$

where TiO_2 and TiO are titanium (IV) and (II) oxides, $Ti-O_x$ is the Ti–O alloy overlayer $(0<x<0.49)$, and the Si atoms produced are not chemically bound within the Hf or Ti layers (for example, Si can stay at the interface as an amorphous Si layer or reincorporate into the Si substrate, or incorporate into the HfO_2 layer, forming a Hf silicate-like layer at the Hf oxide/Si interface.) Our results indicate that Si atoms incorporate into the HfO_2 layer. This is consistent with the TEM observations by Kim *et al.*[12] who did not detect an amorphous silicon layer at the $Ti/HfO_2/Si$ interfaces. However, they assumed that the Si atoms fully recrystallized into the underlying Si substrate.

Both reactions [Eqs. (2a) and (2b)] are thermodynamically favorable processes in the 298–1100 K temperature range,[39] so a driving force exists for the reduction of SiO_2 and formation of titanium oxides. The standard Gibbs free energy change associated with Ti–O alloy overlayer formation, reaction (3), can be calculated by subtraction of the standard Gibbs free energy of SiO_2 formation from its elements[39] from the Gibbs free energy of the interstitial alloy (O in α-Ti) formation $(\Delta G^o_{f,TiO_x})$:

$$\Delta G^o_{f,TiO_x} = \frac{RT}{2}\int_0^x \ln p^{eq}_{O_2} dx, \tag{4}$$

where R is the gas constant, T is the absolute temperature, and $p^{eq}_{O_2}$ is the equilibrium vapor pressure of oxygen above α-Ti for varying dissolved oxygen concentration, according to the reaction $Ti+x/2\ O_2=TiO_x$. An empirical equation given by Wang and Kim[40] can be used to find $\ln p^{eq}_{O_2}$:

$$\ln p^{eq}_{O_2} = 21.24 + 12.45x + 2\ln\frac{x}{1-x} - \frac{131\,200}{T}. \tag{5}$$

The standard Gibbs free energy change of the reaction (3) is negative for all values of oxygen solubility in Ti $(x<0.49)$ and at all temperatures used in our study. Comparison of the reactions (2) (Ti oxide formation) and (3) (alloying) indicate that formation of a Ti–O alloy reaction has lower Gibbs free energy at room temperature, whereas TiO_2 oxide formation dominates at $T>600$ K, $x>0.4$.

The formation of Ti–Si–O phases in the near-surface layer for the crystalline hafnium oxide films is an intriguing finding. As Ti and Si are separated by the hafnium oxide layer, the reaction between Ti and Si can proceed either by

(1) Si up diffusion through the hafnium oxide layer and Si reaction at TiO/HfO_2 interface and in the TiO layer $[5Si+2TiO=2TiSi_2+SiO_2,\ \Delta G^o_{600\ K}=-93.69$ kJ/mol; $3Si+TiO_2=TiSi_2+SiO_2,\ \Delta G^o_{600\ K}=-97.42$ kJ/mol (Ref. 41)] or
(2) Ti diffusion through the HfO_2 layer toward Si substrate, Ti reaction at the HfO_2/Si interface $[Ti+2Si=TiSi_2,\ \Delta G^o_{600\ K}=-130$ kJ/mol, $Ti+2SiO_2=TiSi_2+2TiO_2,\ \Delta G^o_{600\ K}=-195$ kJ/mol (Ref. 39)], and propagation of the $TiSi_2$ and TiO_2 phases through HfO_2 layer toward the surface. Room temperature surface oxidation of Ti silicide produces a mixture of TiO_2 and SiO_2.[42,43]

Both interfacial reactions are possible; hence, the Ti and Si diffusivities also have to be considered. The data on Ti or Si diffusion in HfO_2 are not available. For n-TiO_2, fast Ti cationic diffusion $(D_0=2\times10^{-6}\ m^2/s)$ has been reported, with activation energies of 2.1–2.8 eV.[44] The Ti diffusivities[45] in TiO_2 are similar to values extrapolated for the Hf diffusion in TiO_2 based on the work by Hoshino *et al.*[44] There was no self-interstitial diffusion enhancement at the grain boundaries reported for Ti diffusion in TiO_2, com-

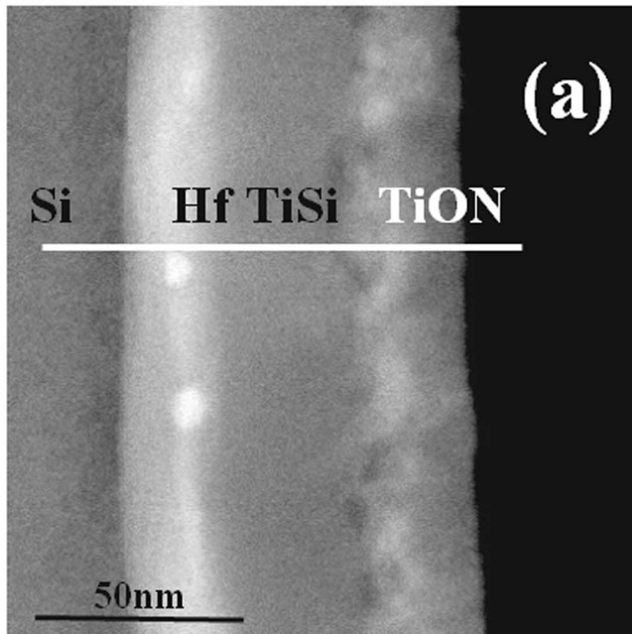

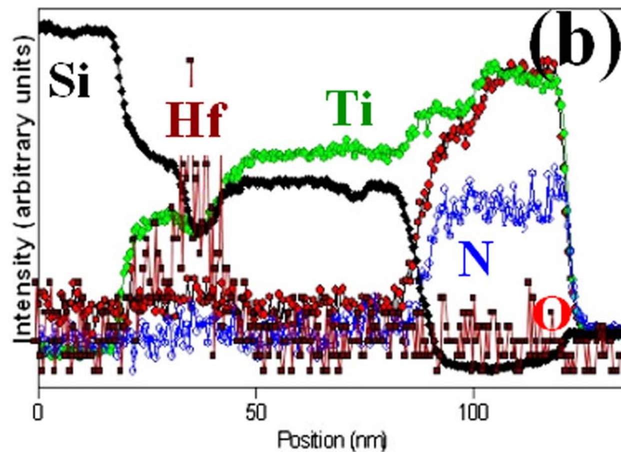

FIG. 7. (a) High angular ADF-STEM image and (b) corresponding EELS/EDXS spectra along the line shown. The thicknesses of the TiSiHf, TiSi, and TiN layers measured from the EELS profile are 26.0–26.5 nm, 27.5–28.0 nm, and 33.0–33.5 nm, respectively. The EELS data clearly indicate the presence of both Ti and Si in the Hf layer, and presence of Si above Hf layer. Note O depletion from Hf-containing layer.

pared to bulk crystallite diffusion. On the other hand, diffusion of Si, based on P and other dopant diffusivities in $HfSi_xO_yN_z$ films,[46] is slow $[D_0=(2-10)\times 10^{-15}\ m^2/s]$. Enhanced dopant diffusion in Hf silicates was attributed to grain-boundary formation resulting from Hf silicate phase separation during annealing. While Ti diffusion is faster according to the literature data, it does not explain the fact that interdiffusion happens only for crystallized HfO_2 films. The MEIS Ti profile (Fig. 4) indicates that there is no significant spread of Ti into the bulk after 600 °C annealing.

The observed surface roughness in the AFM topography data [Fig. 5(b)] indicates that this diffusion process is correlated with the defects in the crystallized HfO_2 layer, possibly

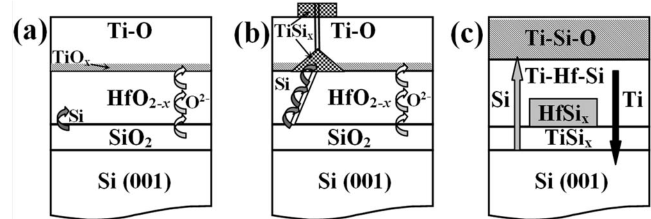

FIG. 8. Schematic showing the proposed O, Si, and Ti diffusion processes across (a) as-deposited, (b) crystallized HfO_2, following the interfacial SiO_2 reduction after 600 °C annealing, (c) after 1000 °C annealing.

the grain boundaries. Under our experimental conditions, formation of a void in the HfO_2 layer is unlikely, as higher temperatures are typically necessary.[47]

Schematics of the diffusion models are summarized in Fig. 8. For the as-deposited HfO_2 films and low annealing temperatures, oxygen is assumed to diffuse from the interfacial oxide through the hafnium oxide layer by a lattice exchange mechanism. The interfacial SiO_2 layer is then eliminated, and a Ti–O overlayer is formed. The hafnium oxide layer also shows partial oxygen depletion. Hf diffusion and reaction at the interface with Si cannot be completely excluded. Hf movement into the interfacial SiO_2 layer after high temperature annealing was observed in similar $TiN/HfO_2/SiO_2/Si$ stacks.[9] There is a shoulder on the lower energy edge of MEIS Hf peak, which may be indicative of this Hf diffusion process. However, the existence of roughness of the top surface does not allow for an unambiguous interpretation.

For the cryst-$HfO_2/SiO_2/Si$ stack, in addition to oxygen transport, Si diffuses and reacts with the Ti layer, forming $TiSi_x$ islands, and, alternatively, Ti diffuses toward Si. Ti diffusion becomes more prominent after 1000 °C annealing. The $TiSi_x$ islands become a $TiSiO_y$ phase when exposed to the air. These Ti silicate islands grow through the flat Ti oxide layer, as suggested by the AFM profile. As a Ti silicate phase formation and an inhomogeneous phase separation on the surface are observed *only* for the cryst-$HfO_2/SiO_2/Si$ stacks, after Ti metallization and 500–600 °C annealing, we suggest that Si diffusion is correlated to the defects in crystallized HfO_2 layers.

V. CONCLUSIONS

We have shown that the interfacial SiO_2 layer thickness in a $HfO_2/SiO_2/Si$ gate stack is reduced, in some cases with low temperature annealing, following deposition of a Ti overlayer, which is known to have a high solubility for oxygen. The HfO_2 layer itself may also be reduced. Si atoms initially present in the interfacial SiO_2 layer incorporate at the bottom of the high-κ layer. Crystallization of the HfO_2 film permits significant Ti–Si interdiffusion through the high-κ dielectric layer and Ti–Si phase formation, tentatively proposed to occur via HfO_2 defects in the crystalline structure, for example, grain boundaries.

ACKNOWLEDGMENTS

The authors thank the SRC, Sematech, the NSF, and CAPES (Brazil) for financial support.

[1]D. Lim, R. Haight, M. Copel, and E. Cartier, Appl. Phys. Lett. **87**, 072902 (2005).
[2]J. K. Schaeffer *et al.*, J. Vac. Sci. Technol. B **21**, 11 (2003).
[3]Z. Chen, V. Misra, R. Haggerty, and S. Stemmer, Phys. Status Solidi B **241**, 2253 (2004).
[4]H. N. Alshareef, P. Majhi, M. A. Quevedo-Lopez, R. Jammy, B. H. Lee, and P. Kirsch, Future Fab International **21**, 98 (2006).
[5]D. G. Schlom and J. H. Haeni, MRS Bull. **27**, 198 (2002).
[6]M. Copel and M. C. Reuter, Appl. Phys. Lett. **83**, 3398 (2003).
[7]K. Xiong, J. Robertson, M. C. Gibson, and S. J. Clark, Appl. Phys. Lett. **87**, 183505 (2005).
[8]E. J. Preisler, S. Guha, M. Copel, N. A. Bojarczuk, M. C. Reuter, and E. Gusev, Appl. Phys. Lett. **85**, 6230 (2004).
[9]M. P. Agustin, L. R. C. Fonseca, J. C. Hooker, and S. Stemmer, Appl. Phys. Lett. **87**, 121909 (2005).
[10]M. Copel, R. P. Pezzi, D. Neumayer, and P. Jamison, Appl. Phys. Lett. **88**, 072914 (2006).
[11]C. S. Park, N. Moumen, J. H. Sim, J. Barnett, B. H. Lee, and G. I. Bersuker, Appl. Phys. Lett. **87**, 253510 (2005).
[12]H. Kim, P. C. McIntyre, C. O. Chui, C. Saraswat, and S. Stemmer, J. Appl. Phys. **96**, 3467 (2004).
[13]P. S. Lysaght, J. J. Peterson, B. Foran, C. D. Young, G. I. Bersuker, and H. D. Huff, Mater. Sci. Semicond. Process. **7**, 259 (2004).
[14]M. P. Agustin, G. Bersuker, B. Foran, L. A. Boatner, and S. Stemmer, J. Appl. Phys. **100**, 024103 (2006).
[15]P. D. Kirsch *et al.*, J. Appl. Phys. **99**, 023508 (2006).
[16]S. V. Ushakov *et al.*, Phys. Status Solidi B **241**, 2268 (2004).
[17]R. M. Tromp, M. Copel, M. C. Reuter, M. Horn von Hoegen, J. Speidell, and R. Koudijs, Rev. Sci. Instrum. **62**, 2679 (1991).
[18]J. F. Ziegler and J. P. Biersack, SRIM, the stopping and range of ions in matter, Version 2003.20, 2003.
[19]K. van Benthem *et al.*, Appl. Phys. Lett. **87**, 034104 (2005).
[20]S. J. Pennycook and L. A. Boatner, Nature (London) **336**, 565 (1988).
[21]K. Xiong, J. Robertson, and S. J. Clark, J. Appl. Phys. **99**, 044105 (2006).
[22]*Binary Alloy Phase Diagrams*, 2nd ed. (ASM International, Materials Park, OH, 1990), Vol. 2, pp. 232–233.
[23]"Ti–Ox" composition notation is used for Ti–O alloy to differentiate from TiO_x oxide formation.
[24]J. T. Mayer, U. Diebold, T. E. Madey, and E. Garfunkel, J. Electron Spectrosc. Relat. Phenom. **73**, 1 (1995).
[25]U. Diebold and T. E. Madey, Surf. Sci. Spectra **4**, 227 (1998).
[26]R. L. Kurtz and V. E. Henrich, Surf. Sci. Spectra **5**, 182 (1998).
[27]Y. Mizuno, F. K. King, Y. Yamauchi, T. Homma, A. Tanaka, Y. Takakuwa, and T. Momose, J. Vac. Sci. Technol. A **20**, 1716 (2002).
[28]J. Domaradzki, D. Kaczmarek, E. L. Prociow, A. Borkowska, R. Kudrawiec, J. Misiewicz, D. Schmeisser, and G. Beuckert, Surf. Coat. Technol. **200**, 6283 (2006).
[29]*Advances in Catalysis*, edited by D. D. Eley, O. H. Werner, and B. Gates (Academic, San Diego, 1996), Vol. 41, p. 271.
[30]M. J. Guittet, J. P. Crocombette, and M. Gautier-Soyer, Phys. Rev. B **63**, 125117 (2001).
[31]T. L. Barr, J. Vac. Sci. Technol. A **9**, 1793 (1991).
[32]C. D. Wagner, A. V. Naumkin, A. Kraut-Vass, J. W. Allison, C. J. Powell, and J. R. Rumble, Jr. (National Institute of Standards and Technology, 2003), Vol. 2006.
[33]B. W. Busch, W. H. Schulte, E. Garfunkel, T. Gustafsson, W. Qi, R. Nieh, and J. Lee, Phys. Rev. B **62**, R13290 (2002).
[34]A. S. Foster, A. L. Shluger, and R. M. Nieminen, Phys. Rev. Lett. **89**, 225901 (2002).
[35]J. L. Gavartin (private communication).
[36]Y. Wang, M.-T. Ho, L. V. Goncharova, L. S. Wielunski, S. Rivillon, R. T. Brewer, Y. J. Chabal, and T. Gustafsson, Chem. Mater. (submitted).
[37]J. C. Barbour, A. E. M. J. Fischer, and J. F. van der Veen, J. Appl. Phys. **62**, 2582 (1987).
[38]M. Liehr, F. K. LeGoues, G. W. Rubloff, and P. S. Ho, J. Vac. Sci. Technol. A **3**, 983 (1985).
[39]I. Barin and O. Knacke, *Thermochemical Properties of Inorganic Substances* (Springer, Berlin, 1977).
[40]W. E. Wang and Y. S. Kim, J. Nucl. Mater. **270**, 242 (1999).
[41]R. Beyers, R. Sinclair, and M. E. Thomas, J. Vac. Sci. Technol. B **2**, 781 (1984).
[42]A. Cros, C. Pirri, and J. Derrien, Surf. Sci. **152–153**, 1113 (1985).
[43]R. Pantel, D. Levy, D. Nicolas, and J. P. Ponpon, J. Appl. Phys. **62**, 4319 (1987).
[44]K. Hoshino, N. L. Peterson, and C. L. Wiley, J. Phys. Chem. Solids **46**, 1397 (1985).
[45]U. Brossmann, R. Wurschum, U. Sodervall, and H.-E. Schaefer, J. Appl. Phys. **85**, 7646 (1999).
[46]M. A. Quevedo-Lopez *et al.*, J. Appl. Phys. **97**, 43508 (2005).
[47]P. S. Lysaght, B. Foran, G. I. Bersuker, P. J. Chen, R. W. Murto, and H. R. Huff, Appl. Phys. Lett. **82**, 1266 (2003).